IPM CLAW-POLE ALTERNATOR SYSTEM FOR MORE VEHICLE BRAKING ENERGY RECUPERATION

Lucian TUTELEA, Dragos URSU, Ion BOLDEA, Sorin AGARLITA

Dept. of Electrical Machines &Drives,"Politehnica" University of Timisoara, Bd. V. Pârvan, no.2, Timiş oara, RO

Abstract: *This paper aims to demonstrate that by using permanent magnets (PMs) between the rotor poles, larger air-gap and raised voltage, the hereby called Inter-Polar Magnets (IPMs) Claw-Pole Alternator (CPA) is suitable up to 100 kW peak power for more vehicle braking energy recuperation or propulsion support in HEVs. The main contributions of the paper may be divided into: a comprehensive 3D magnetic circuit for IPM-CPA with magnetic saturation and skin effect considered and its validation through 3D-FEM and some experimental results; optimal design method and code for IPM-CPA; system simulation model and code for a proposed Li-Ion battery backed 42 Vdc "hidden" power bus for 8 kW peak power of vehicle braking energy recuperation; decoupled control of 42 Vdc Li-Ion battery and dc-dc converter control of 14 Vdc loads is demonstrated for up to 5 kW load levels. The encouraging results obtained so far are hoped to be a sounder basis towards more braking energy recuperation on automobiles for further gas mileage improvements with moderate initial costs.*

Key words: *3D-FEM, claw-pole alternator design and control, interior permanent-magnet, optimal design, energy recuperation*

1. Introduction

The alternator is an electromechanical energy conversion device designed to take mechanical energy from the internal combustion engine ICE (through the stored magnetic energy in the air-gap of CPA) in order to supply with electrical energy all the vehicle electric loads [1]. In a Lundell machine (CPA) the energy conversion has a low efficiency (especially at high speeds), between 40% and 70% [2].

The claw-pole alternators (CPAs) are capable of producing power densities notably larger than the conventional machines [3]. But the CPA is characterized by: high saturation, high magnetic leakage between claws (about 30-40% of the main flux), low efficiency and relatively large field time constant [4, 5]. The rotor consists of forged pole pieces (claw poles) secured around a circular field coil (Fig. 1). Regulating the field current controls the alternator system diode – rectified output voltage.

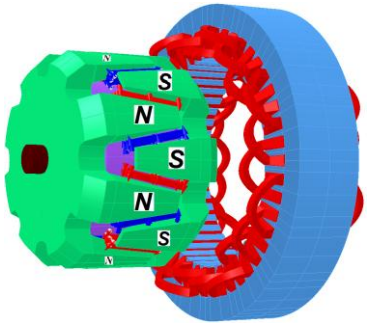

Fig.1. The geometry of the IPM-CPA (from 3D FEM analysis)

To minimize cost, single layer stator windings, with q=1 (one slot per phase per pole) are used.

The electric power demands on conventional vehicle are increasing because many devices driven directly by the engine are being proposed to be driven electrically in order to improve the vehicle energetic efficiency and to reduce the pollutant emission [6]. The new electric accessories on automobiles (electric drives for air conditioner, power steering assist, various ventilators, fuel pump, etc.) require increased average (and peak) electric power from on board alternator, pushing the alternator to its limits [4].

The studies performed by Perreault, Caliskan and Whaley have investigated means of extracting more electrical power from the Lundell alternator using the switched-mode rectifier (SMR) [4, 7, 8]. Introducing a SMR increases the power at 14 Vdc by a factor of 2 at 42 Vdc, while the efficiency increases from 40% to 60% at 6000 [rpm] [7], but the SMR additional cost has to be considered. A recent in-depth study of SMR is to be found in Ref. [9].

Using a booster diode, in fact a four leg three-phase rectifier, can increase the efficiency of the alternator by 1% and power output of the alternator by 10 % (only at high speeds) [1]. A more complex solution that ensures a power increase at all speeds is assisting PMs [1]. Surface PMs produce notably larger DC output current, but unfortunately, only at higher speeds. Placing the PM between poles gives better performance on the whole speed range. Inserting PMs in the inter-polar regions will provide magnetic flux that will reduce flux leakage between two successive rotor poles [10].

The idea to improve the vehicle energetic performance by recovering some of the braking energy is already used in the electric vehicles [6, 11], but it was proposed [12] recently on conventional vehicles, combined with a proper energy management [13-14].

Efficient distribution of a large power in terms of costs and losses require larger dc bus voltage. The 42 Vdc bus was chosen as a compromise between power distribution efficiency and passenger safety [15].

Sections II-V of this paper introduce a methodology and results from the optimal design of a 3.2 kW claw-pole alternator and from a three dimensional Finite Element Analysis (3D-FEA), at no-load and load operation conditions. A modified Bosch alternator is analyzed (using magnetic equivalent circuit (MEC) and 3D-FEM), showing that a short-time braking power of 8 kW can be recovered if the voltage is increased three times (form 14 Vdc to 42 Vdc) and inter-polar magnets (IPM) are used.

Sections VI-VIII deal with the control of IPM-CPA with a braking energy recuperation "hidden" 42 Vdc power net and finally adds a study on extension of the power range of IPM-CPA to 100 kW. As the proposed solution is producing most of the electrical power during the vehicle braking by recovering a part of its kinetic energy, the alternator and rectifier efficiency are not so important at their highest power since the storage capacity is much smaller than vehicle kinetic energy. This way the alternator mass and its cost are still reasonable. However, in avoiding overheating of IPM-CPA , good efficiency is needed. Also high efficiency is needed at lower power (normal) loads. Most of existing loads remain on the existing lead acid battery [16], connected to the 42 Vdc power net bus through a buck chopper while New, high power, consumers (such as the electrically driven air conditioner) may be connected directly to 42 Vdc "hidden power" bus through their embedded power electronics [17-18]. A case study system simulation in MatLab-Simulink is presented and discussed.

2. 3D Nonlinear Magnetic Circuit Model

The optimal design of the IPM-CPA is based on the magnetic equivalent circuit (MEC) and Hooke-Jeeves modified algorithm [19, 20, 21]. In the MEC method, each region of the machine is represented by a permeance whose value depends on local geometrical quantities and on the local geometry and/or flux through the region.

The mathematical model of a claw-pole machine is complicated because the paths of the magnetic flux are 3D. Each flux path section is characterized by a magnetic reluctance.

For all these magnetic reluctances analytical expressions have been adopted [1]. The MEC of the IPM-CPA (Fig. 2) is a three-dimensional model in the sense that the permeances of air-gap, of stator and of rotor vary along radial, axial and tangential directions. The presence of IPMs on rotor is also considered in the MEC.

The MEC model is used for the optimization of the machine using a non-linear iterative method based on the linearization of the B-H curve [20].

The dynamic characteristics of the machine can be studied by rotating the rotor mesh with respect to the stator. When the rotor is rotated the radial and axial air-gap reluctances, together with the axial leakage paths between the claw-poles and the plates, are modified accordingly.

The details of MEC composition are skipped here to save space.

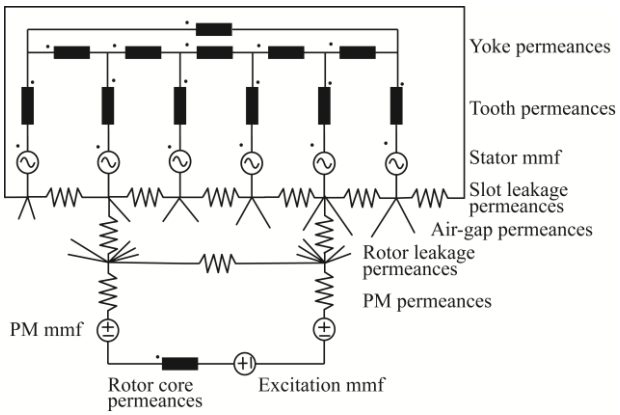

Fig.2. Multiple MEC of the IPM-CPA (one pole pair)

3. Evaluation Design Calibration

The described MEC model had to be checked before proceeding to optimization design, finite element analysis and control.

For this purpose a 14 Vdc, 2.5 kW Bosch claw pole alternator without IPMs has been used. A good agreement between simulation and experiment can be seen both in Fig. 3 (where the efficiency has been plotted) and in Fig. 4 (where the maximum dc current has been plotted). Based on these results we concluded that the MEC model is precise enough to continue the analysis of CPA through it.

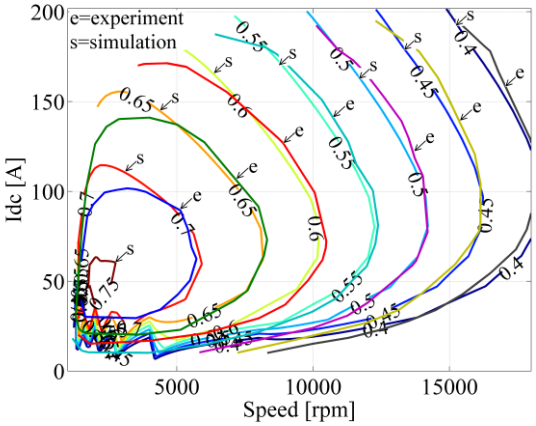

Fig.3. Efficiency of a 2.5 kW, 14 Vdc CPA without IPM

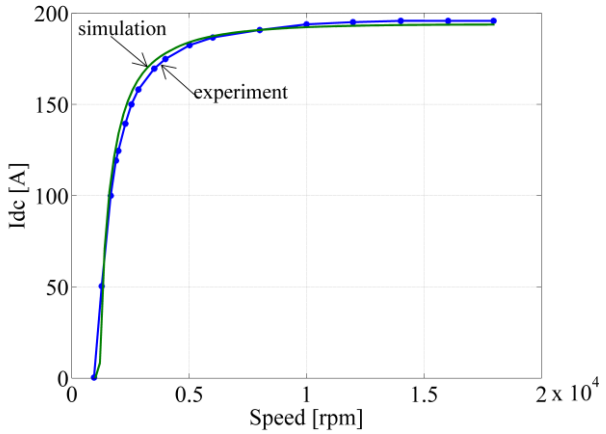

Fig.4. Maximum dc current of a 2.5 kW, 14 Vdc CPA without IPM

4. Optimal Design: Method, Code and Sample Results

The modified Hooke-Jeeves optimization algorithm is used in order to allow constrained system optimization using external penalty functions.

The complete analytical model has been written in MatLab, being structured in m-files.

The objective function represents the total (initial plus losses) cost and has the most important parameters as variables. This function will be minimized using the Hooke-Jeeves algorithm.

The optimized variables are grouped in the vector $\bar{X}$:

$\bar{X}$ =[sDo, sDi, rDci, lc, shy, stw, sMs, hag, poles, sb, ap, rpl, wrd, lrc, rdcl, rph, Iextmax, kipm].

The eighteen optimization variables are explained in table 1.

For the 3.2 kW rated power and 8 kW peak power at 42 Vdc, the values (in mm) of their initial dimensions are:

$\bar{X}$ =[151, 106, 54, 37, 7, 3, 2.8, 0.8, 16, 8, 0.82, 37, 14.4, 54.8, 5.4, 10, 2800, 0.5]

This optimization vector varies in a range, between $\bar{X}_{min}$ and $\bar{X}_{max}$ ($\bar{X}_{min} < \bar{X} < \bar{X}_{max}$).

The chosen lower and upper limits are:

$\bar{X}_{min}$ = [100, 75, 35, 25, 3, 3, 2.5, 0.3, 4, 2, 0.6, 15, 7, 25, 1 4, 500, 0]

$\bar{X}_{max}$ =[330, 230, 130, 80, 20, 20, 8, 2, 32, 20, 0.9, 80, 40, 150, 18, 20, 5500, 0.9]

The initial step vector (initial variation of the optimization variable) $d\bar{X}$ and the minimum step vector (final variation of the optimization variable) $d\bar{X}_{min}$ are:

$d\bar{X}$ = [16, 16, 10, 5, 2, 1, 0.5, 0.4, 4, 2, 0.1, 5, 2, 10, 2, 2, 500, 0.1]

$d\bar{X}_{min}$ = [0.5, 0.5, 0.5, 0.5, 0.1, 0.1, 0.1, 0.05, 2, 1, 0.01, 0.1, 0.1, 0.1, 0.1, 0.1, 20, 0.01]

The program achieves a minimum of the objective function after around 70 steps.

Table 1.
Optimization variables of the IPM-CPA

sDo	Stator outer diameter
sDi	Stator inner diameter
rDci	Rotor coil inner diameter
lc	Stator core length
shy	Stator core yoke width
stw	Stator tooth width
sMs	Mouth of stator slot
hag	Air-gap length
poles	Number of poles
sb	Turns per coil
ap	Polar cover
rpl	Rotor pole length
wrd	Width of rotor end disk
lrc	Rotor core length
rdcl	Rotor core length variation due disk
rph	Rotor pole height
Iexmax	Maximum [A turns] do field coil
kippm	Inter pole PM: 0 –no IPM

The resulting optimized vector (from which the 3D-FEM analysis will start) is:

$\bar{X}_0$ = [164, 107, 53.5, 34.5, 12.8, 3, 3.1, 0.4, 16, 8, 0.81, 34.3, 13.4, 70.5, 4.2, 10, 2780, 0.49]

The optimization reveals that a maximum braking output power of 8 kW is achievable into the frame of a 3.2 kW, 14 Vdc CPA, after it is redesigned for 42 Vdc (Fig. 5). The efficiency of the IPM-CPA has increased by 5% by optimization (a very practical initial design variable vector was chose) , from 80 % to 85 % (Fig. 5). This is 10% higher than the efficiency achieved in a 2.5 kW, 14 Vdc alternator (without IPMs).

An experimental 42 Vdc IPM-CPA has been built by Robert Bosch GmbH within the FP7 EE-VERT 2009-2011 European program in which the authors are involved. The experimental results (Fig. 6) show a maximum efficiency of 80% and a maximum braking output power of 11 kW.

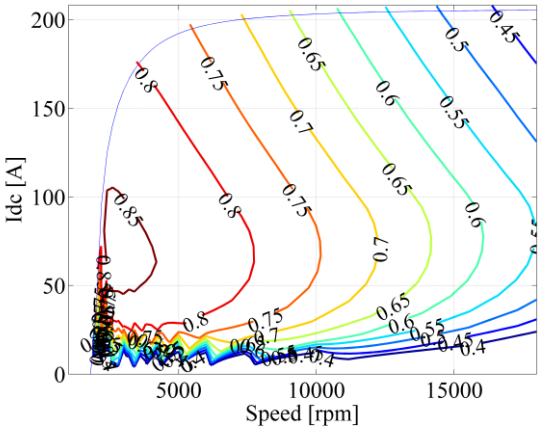

Fig. 5. Efficiency of the optimized IPM-CPA at 42 Vdc

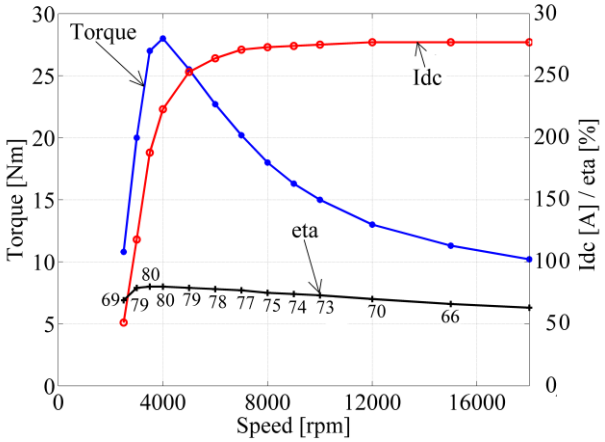

Fig.6. Experimental results of a retrofited Bosch 3.2 kW, 42 Vdc IPM-CPA

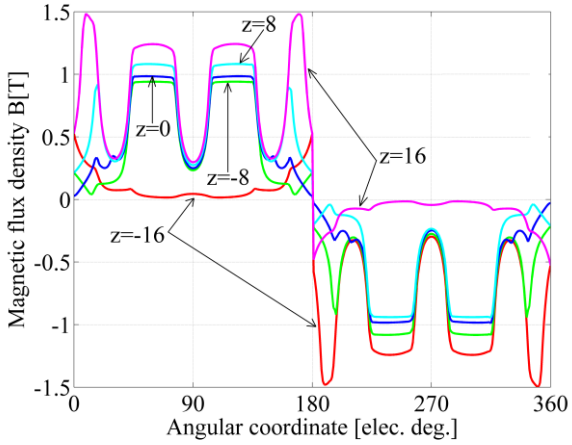

Fig.7. Distribution of the magnetic flux density at no load-IPM-CPA (D.C. field m.m.f. = 1500 [At]) at different axial lenghts: z=-16; -8; 0; 8; 16 [mm]

5. 3D FEM Analysis

FEM is a valuable tool in the final stage design verifications, where it is used to check the saturation level and air-gap magnetic flux density waveform at steady state. Due to the high number of elements compared to MEC, FEM offers higher accuracy. The magnetic flux flows through the claw-poles and rotor yoke in z-direction, therefore 3D FEM analysis is mandatory.

The variable that is solved in an electromagnetic FE problem is the magnetic potential at the nodes of the elements. All the important quantities can be obtained by applying differential operators to magnetic vector potential [23].

The FE model of the 16 poles IPM-CPA (Fig. 1) was implemented in a commercial software package by means of the built-in script programming [23]. In the FEA, the demagnetizing curve of the NdFeB IPM (VAC 677 type) was taken into account. They have a remanent flux density Br (at 20º C) equal to 1.13 [T] and a coercive field strength (at 20º C) of 8.6·105 [A/m].

All the dimensions were imported from the MEC optimal design of the IPM-CPA ($\bar{X}_0$).

Studying Fig. 7 we can gain better understanding of the magnetic flux density in the airgap of an IPM- CPA. Only at axial distance z=0 (in the middle) the magnetic flux density has a symmetrical variation when we move from one pole to another.

The influence of slot opening in the magnetic flux density at no load operation is evident. The strong departure of the air-gap flux density distribution from a sinusoidal waveform is due to the low number of slots per pole (3), and to magnetic saturation [1]. The air-gap magnetic flux density harmonics are responsible for induced e.m.f.'s harmonics "pollution". Also, air-gap field harmonics produce additional eddy currents in the claw poles. These losses increase with speed [5].

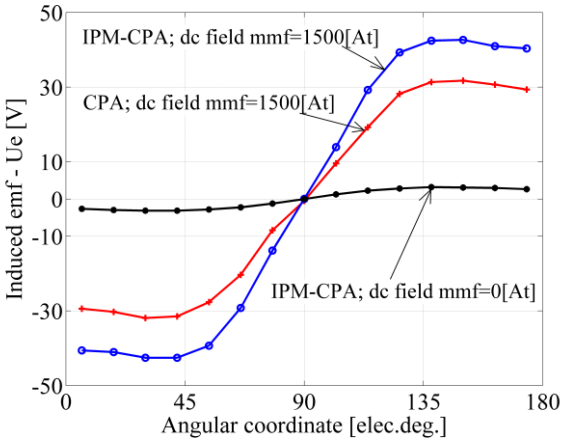

Fig. 8. Computed e.m.f. in a stator phase at 3000 [rpm]

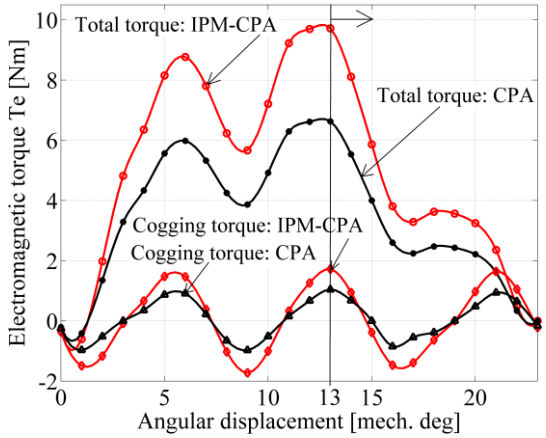

Fig.9. Total and cogging torque at Imax=Ia= -2Ib= -2Ic=200[A]

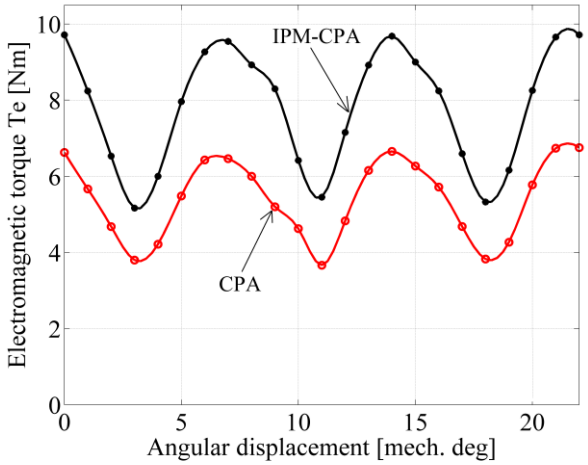

Fig. 10. Torque pulsation of the CPA

To find the flux through a stator coil, a surface corresponding to the coil geometry was defined. The script rotates the mobile part with a step of 1.5 mechanical degrees over one pole, analyses the model and computes the integral of magnetic flux density over the defined surface. Given the Faraday law: derivating the flux with respect to the mechanical angle and multiplying it by speed (and all the other transformation constants) we obtain the e.m.f. induced at no-load in a phase (Fig. 8). The e.m.f. induced only by the IPM at 3000 rpm is about 3 V (peak value).

This value assures us that even at maximum alternator speed (18000 rpm) the no load voltage (18 V peak, per phase), at zero field current presents no threat to power electronics equipment.

The torque was computed using Maxwell stress tensor. At constant stator currents: Ia=Imax, Ib= -Imax/2, Ic= -Imax/2, the rotor is rotated along a pole with a step of 1 mechanical (8 electrical) degree. The maximum stator current is the one from optimization design, Imax=223A at d.c. field m.m.f of 2800 A·turns. This gives us the total torque in Fig. 9 .The camel-back shape of the total torque is due the "cogging" torque (Fig. 9), which appears because the interaction between the stator teeth and magnetized rotor, when the field current and IPMs are present.The torque pulsations in total torque (Fig. 10) were obtained by modifying the three sinusoidal stator currents: Ia, Ib and Ic with respect to the angular shifting of the rotor for a given dq power angle and initial rotor angle of 104˚ (13˚×8) (Fig. 9)- which should correspond to unity power factor operation due to diode rectifier constraint. The average value of the torque of the CPA with IPM is 7.8 [Nm], while the average torque value for the CPA without IPM is about 5.1[Nm]. More than 40 % torque increase is obtained by PMs. (The Bosch modified IPM-CPA in Fig. 6 is not exactly our optimized design which explains its higher power range, but confirms the rising torque trend).

6. Vehicle Braking Energy Recuperation Scheme and its Control

The proposed vehicle power net (Fig. 11) for vehicle braking energy recuperation, contains the electrically excited claw pole alternator, with its embedded diode rectifier, the storage Li-ion battery with high voltage loads, the lead acid battery with classical low voltage loads and two dc-dc quadrant converters, one to interconnect the 42 Vdc bus with the14 Vdc bus and the second to supply the excitation circuit of the alternator. This architecture has the advantage to preserve the actual power bus structure for existing loads and at the same time, to offer a larger voltage for new high power consumers as air-conditioners and other new electrical actuators.

The power converter supplies only the 14 Vdc loads so its cost and power level and losses are reduced. The 14 Vdc dc bus experiences less influence of the engine speed variation and, consequently, its level is more stable.

The energy management block is controlling the alternator excitation current in order to extract the maximum calculated power of 8÷11 kW, sufficient in vehicle urban driving to reduce fuel consumption by 8÷10 %, if the battery state of charge (SOC) is smaller than unity. Respectively, to produce power between zero and maximum load required (according to battery SOC) when the vehicle is not braking.

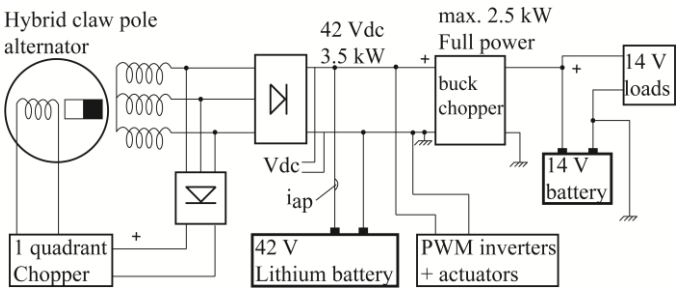

Fig. 11. Vehicle power net

A. *Dynamic model of the proposed system*

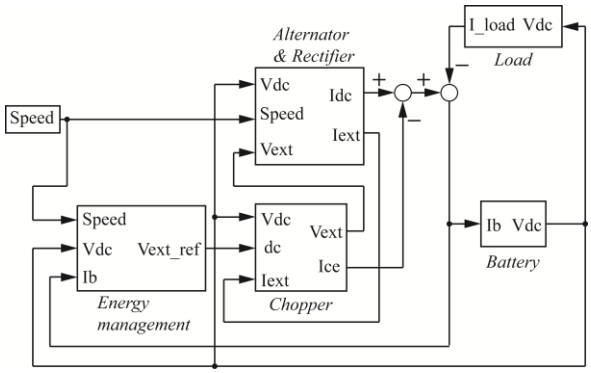

Fig. 12. Power net Simulink model

The MatLab-Simulink model of power net is reflecting its structure in Fig. 12, containing the alternator with embedded rectifier model, storage battery model, load model, excitation circuit model and the energy management block. The alternator speed, that is in direct relation with the vehicle engine speed, is the input variable of the simulations.

The main element of the power net is the new alternator capable to produce maximum power (during the vehicle braking) which should be installed in less than 0.1s because the duration of one braking period is only a few seconds. The model of alternator is based on the dq equations that handle dc variables in steady state. Usually the dq variables (currents and voltage) are linked to the phase components through the Park transformation and then, through the rectifier, to the dc bus. The alternator current is rather sinusoidal at working frequency (400-800 Hz for a 3000 to 6000 rpm) despite the diode rectifier, and, consequently, the dominant power transfer is through the fundamental harmonic.

A simple algebraic equation could be used between phase voltage and dc bus voltage, respectively, phase's current and dc bus current [24]. The alternator fundamental voltage is considered in phase with its current and, using the relation between phase voltage/currents and dc bus voltage/currents, it is possible to use directly the reduced value of the dc voltage (1) in the dq model, and also to compute directly the dc current from dq currents (3).

$$V_m = k_v \; V_{dc} - 2V_d \tag{1}$$

here: V_m – the d, q model voltage vector magnitude,
V_{dc}– dc voltage,
V_d– direct voltage drop on the diode,
k_v– dc voltage reduction factor (2):

$$k_v = \begin{cases} \frac{2}{\pi} & \text{for star widings connection} \\ \frac{2}{\pi}\sqrt{3} & \text{for delta widings connection} \end{cases} \tag{2}$$

$$I_{dc} = k_i \sqrt{I_d^2 + I_q^2} \tag{3}$$

where: - Idc – the dc alternator current,
Id– d axis current component,
Iq– q axis current component,
k_i– stator current reduction factor (4):

$$k_v = \begin{cases} \frac{3}{\pi} & \text{for star widings connection} \\ \frac{3}{\pi}\sqrt{3} & \text{for delta widings connection} \end{cases} \tag{4}$$

Permanent magnets are placed between claw poles in order to reduce the excitation field fringing. A small PM flux appears in d axis in the same direction with the excitation flux but the main benefit of PMs is the improvement of excitation characteristics. Finally the alternator dq voltage equations are presented in (5, 6) while the excitation equation, reduced to the stator winding appears in (7). The transformer coupling between stator d axis and excitation flux appears also between time I_d, I_{e1} derivatives (8).

$$\frac{d\Psi_d}{dt} = -V_m \sin\ \theta\ - k_s R_s I_d + \omega_e L_q I_q \tag{5}$$

$$\frac{d\Psi_q}{dt} = -V_m \cos\ \theta\ - k_s R_s I_q + \omega_e\ \ \Psi_{PM} + I - \omega_e L_q I_q \tag{6}$$

$$\frac{d\Psi_{e1}}{dt} = V_{e1} - R_{e1} I_{e1} \tag{7}$$

$$\frac{d}{dt}\begin{pmatrix} I_d \\ I_{e1} \end{pmatrix} = \begin{pmatrix} L_d & -L_{md} \\ -L_{md} & L_{e1} \end{pmatrix}^{-1} \cdot \begin{pmatrix} \frac{d}{dt}\Psi_d \\ \frac{d}{dt}\Psi_{e1} \end{pmatrix} \tag{8}$$

where: Ψ_d – d axes flux,
Ψ_q – q axes flux,
Ψ_{e1} – excitation stator reduced flux,
R_s – dc stator winding resistance,
k_s – skin effect factor,
L_d – d axes inductance,
L_q – q axes inductance,
L_{md} – d axes main inductance,
V_{e1}– excitation reduced voltage,
I_{e1} – excitation stator reduced current,
R_{e1} – excitation stator reduced resistance,
L_{e1}– excitation stator reduced inductance,
ω_e – electric speed,
θ – internal angle (between voltage vector and q axis

The currents are computed by integrating their derivatives from (8) and (6), but the integration results are limited to positive values to consider the embedded rectifier in the stator and the one quadrant chopper in the excitation. When either the excitation current or d axis current is zero (smaller than a positive given error in the simulation) decoupled circuits are considered (9):

$$\frac{d}{dt}\begin{pmatrix} I_d \\ I_{e1} \end{pmatrix} = \begin{pmatrix} \frac{1}{L_d} & 0 \\ 0 & \frac{1}{L_{e1}} \end{pmatrix} \begin{pmatrix} \frac{d}{dt}\Psi_d \\ \frac{d}{dt}\Psi_{e1} \end{pmatrix} \tag{9}$$

The internal angle θ is the current vector angle with axis q (the voltages are in phase with currents) if either Id or Iq is different to zero; else, θ is the angle of total rotor produced (transformer and rotating) induce voltage (10) with axis q. This "trick" is required to start the diode rectifier action when Id & Iq=0.

$$\theta = \begin{cases} \text{atan}\ I_d, I_q & \text{if } I_d \neq 0 \vee I_q \neq 0 \\ \text{atan}\ V_{e1} - R_{e1} I_{e1}, \omega_e\ \ L_{md} I_{e1} + \Psi_{PM} & \text{if } I_d = 0 \wedge I_q = 0 \end{cases} \tag{10}$$

A simplified empirical skin effect equation (11) is proposed considering the electric speed, ωsk; it leads to almost doubling the ac resistance compared with dc resistance at high speeds. The equation has the merit to consider the skin effect dependence with the frequency at 1.5 exponent at very large frequency while a single parameter, ωsk, should be provided. It shows a good agreement with the standard hyperbolic functions that are considering the slot geometry and conductor diameter, parameters that are not generally available for commercial alternators.

$$k_s = 1 + k_{sk} \frac{\omega_e^{2.5}}{\omega_e + \omega_{sk}}; \qquad k_{sk} = 2\omega_{sk}^{-1.5} \tag{11}$$

The model is computing also the shaft torque that could be used as input for other blocks in complex vehicle dynamic simulation or to compute the alternator efficiency. The shaft torque, TS, (12) has three components: the electromagnetic torque associated to the power transmitted to stator winding, the electromagnetic torque associated to the iron losses and mechanical losses torque.

$$T_s = \frac{3}{2}\left[p\ \Psi_d I_q - \Psi_q I_d\ + p\omega_e \frac{\Psi_d^2 + \Psi_q^2}{R_{Fe}} \right] + T_{f0} + k_f n^2 \tag{12}$$

where: p – number of pole pairs,
R_{Fe} – equivalent iron losses resistance,
T_{f0}– friction torque,
k_f – coefficient of ventilation torque,
n – mechanical speed in rpm.

The discontinuous alternator current mode is not considered in this model because it appears only at low speed and has low influence on the energy balance.

B. 42 Vdc Storage battery model

The Li-Ion 42 Vdc storage battery is an important power net component and a simple battery model, considering the internal constant resistance and a nonlinear battery emf voltage dependence with battery state of charge (SOC), is proposed here (13,14).

$$V_b = R_b I_b + V_{be} \tag{13}$$

$$V_{be} = \begin{cases} V_0 \dfrac{Q}{Q_0} & for\ 0 < Q \le Q_0 \\ V_0 + V_{bn0} - V_0 \dfrac{Q - Q_0}{Q_n - Q_0} & for\ Q_0 < Q \le Q_n \end{cases} \tag{14}$$

where: R_b – battery resistance,
I_b – battery current,
V_{be}– battery emf voltage,
V_{bn}– battery rated emf voltage,
V_0 – emf voltage for discharged battery,
Q – actual battery electric charge,
Q_n – battery rated charge,
Q_0– battery residual charge.

The battery charge is computed by integrating the current and is limited between zero and rated charge as shown in (15) where Q(tk), Q(tk-1) is charge at time tk, respectively, at tk-1 and dt is an infinitesimal time difference between tk and tk-1.

$$Q\ t_k\ = \begin{cases} 0 & \text{if } Q\ t_{k-1}\ + I_b dt \le 0 \\ Q\ t_{k-1}\ + I_b dt & \text{if } 0 < Q\ t_{k-1}\ + I_b dt < Q_n \\ Q_n & \text{if } Q_n \le Q\ t_{k-1}\ + I_b dt \end{cases} \tag{15}$$

The real battery behavior is more complex with temperature dependences, aging, and history of charge discharge cycles but, for our scope here, the simple model it is enough accurate.

C. The control strategy

The load power is assumed constant and the load current is computed considering the dc variable voltage. A low pass filter on the load current simulates the time constant of the load power converter. The energy management block is organized on two hierarchical levels: the battery voltage control and battery current control.

The battery actual emf voltage is computed considering the dc voltage, battery current and battery resistance. The control is based on a monotonically relation between battery emf voltage and battery state of charge. The battery voltage control block (Fig. 13) is the key of the energy recovering and storage energy management and it consists in a variable structure control.

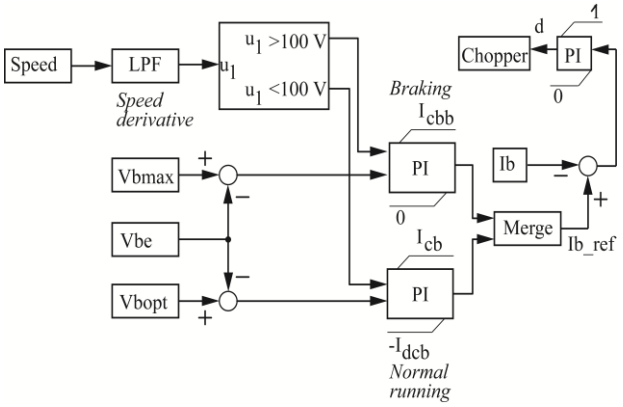

Fig. 13. Battery voltage and current control

The speed derivative is computed and if it is smaller than a certain negative value then the emf battery voltage reference is set at maximum value, Vbmax, otherwise it is set to an optimal value, Vbopt, small enough to secure energy recovering from several repetitive braking, but high enough to supply the vehicle loads a certain time interval when the engine is stopped. In a real vehicle a signal from the braking pedal or from a sudden release of acceleration pedal could be used to change the battery reference voltage in the voltage controller. Both controllers are PI controllers with limitations but with different parameters.

The "Braking" PI controller (Fig. 13) has a larger gain and its upper current limit is set equal to maximum battery charge current and its minimum is zero, while the "Normal running" PI controller (Fig. 13) has a smaller gain, smaller charger current, and the lower limit is negative and it means maximum battery discharging current. The internal states of controllers are frozen when inactive and when the control structure is changed, the active controller starts from the last internal state.

The battery current controller (not shown in a graph) is also a PI controller with limitation and a large frequency band (Fig. 12). Its output between zero and unity (in p.u) represents the duty cycle for the excitation chopper. The chopper model is computing the excitation voltage, Vex , and the required current from excitation, Ich , considering the dc voltage, voltage drop on the chopper device and excitation current from the alternator model (16)-(17).

$$V_{ex} = d \cdot V_{dc} - \Delta V_{ch} \quad (16)$$

$$I_{ch} = d \cdot I_{ex} \quad (17)$$

D. Simulation results

The scope of simulations is to show the controlled alternator capabilities to change quickly its states to follow the required dynamics for braking energy recovery. To this scope, a repetitive alternator speed input signal was considered with an acceleration time from 3000 rpm to 6000 rpm, running time at 6000 rpm, deceleration time at 3000 rpm and running time at 3000 rpm (Fig.14.a).

The alternator parameters are: p=8 pole pairs, Rs =0.0416 Ω, Rex =7.07 Ω, kex =28.2, Lmd =0.26 mH, Lmq =0.21mH, Lse =0.8 H, ΨPM =0.4 mWb, fskr =1003 Hz, Vd =0.65 V, Rfe =5 Ω, winding connection – delta, Tf 0 =0.17 Nm, kf =10-9 Nm/rpm2.

The battery parameters are: Cn =64 Ah, Vn =42 V, V0 =36 V (10% charged), Rb = 0.05 Ω.

The control parameters are: Vbmax =42 V, Vbopt =39 V, Icb =6.5 A (slow charging battery current), Icbb =120 A(maximum battery charge current), Idcb =20 A (maximum battery discharge current).

In the first simulation the load is set at 2.5 kW and the battery SOC is 0.8. The power net evolution is presented for 120 seconds through several key variables as alternator shaft speed Fig. 14.a , excitation Fig. 14.b , alternator Ia and battery current Ib, Fig. 14.c, battery terminal voltage and battery emf, Fig. 14.d & Fig. 14.e.

Three acceleration-deceleration pulses occur during the investigated period. The initial states of controllers are set to zero. They reach the quasi steady state after the first acceleration deceleration cycle, so the behavior of the system is different during the first cycle and then it will be repeated identical for thousands of cycle until the battery emf reaches its reference (39V, assumed to be optimal).

The limitation of the discharge current made the battery emf regulation process slow but it distributed uniformly the recovery energy usage between deceleration periods and limits the battery agging.

A larger value of discharge current lets the system to consume the recovery energy immediately, accelerates the battery discharging process but it will increase the battery aging.

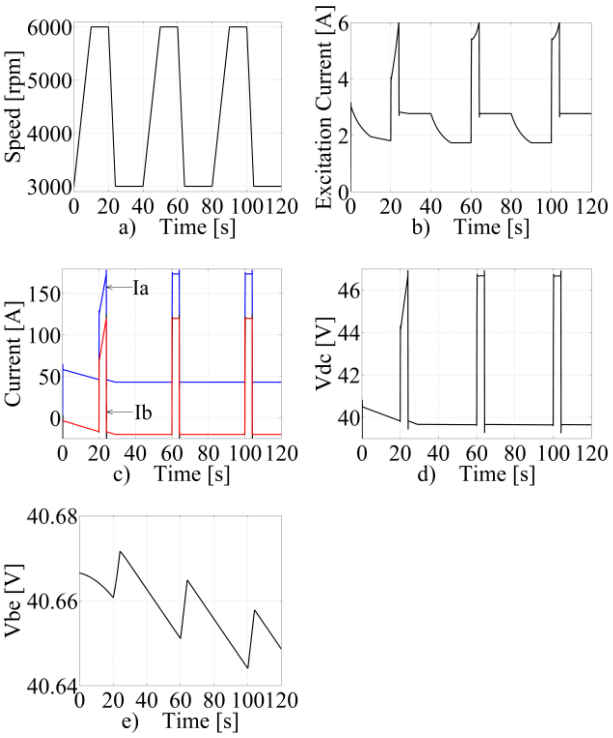

Fig.14. Parameters variation at SOC=0.8, Pload=2.5 [kW]

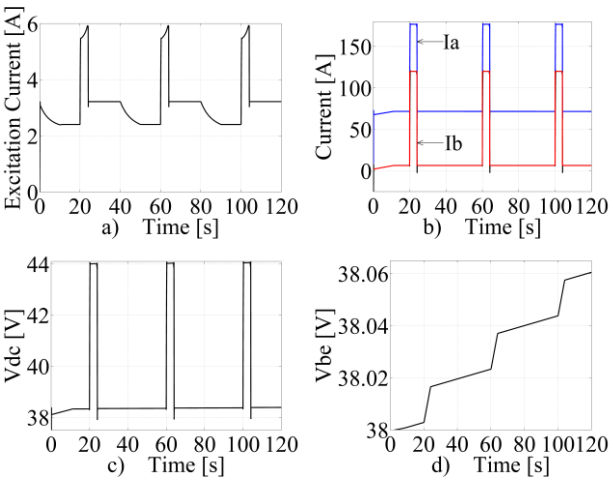

Fig.15. Parameters variation at SOC=0.4, Pload=2.5 kW

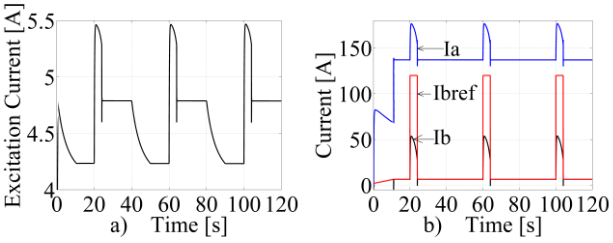

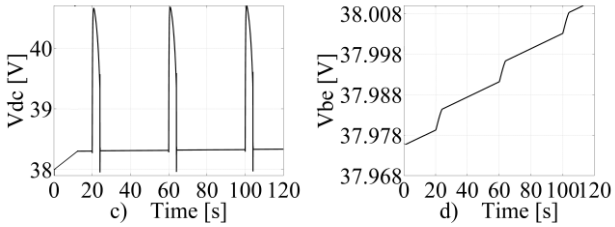

Fig.16. Parameter variation at SOC=0.4, Pload=5 kW

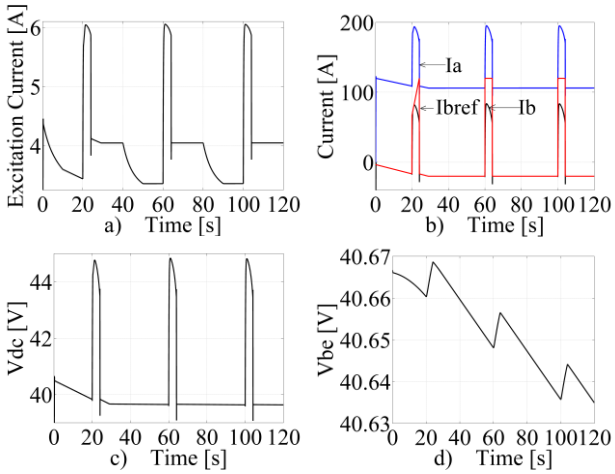

Fig.17. Parameter variation, SOC=0.8, Pload=5 kW

The next simulations, (Fig. 15), that consider a battery initial SOC equal to 0.4, show that the battery charging process is also very slow, so there is no reason to accelerate the discharge process. This behavior is a consequence of larger battery capacity which was chosen considering the maximum permissive recharge current. This is unlike the criterion for super- capacitors sizing, should they be used instead of Li-ion battery which should be based on storage capacity.

The previous simulations show that the alternator has reserve power and it could produce quickly the required power. At the process scale there is no observable difference between reference battery current from voltage controller and real battery current (Fig. 14 and Fig. 15).

The following simulations, (Fig. 16), show the system behavior when the load is increased to 5 kW and the battery initial SOC is 0.4. The battery terminal low voltage is limiting the maximum value of the excitation current and the actual recharging current during the braking is not able to follow the reference current, Fig. 16. b, and the recover energy is smaller. This is proved by lower torque despite of larger power requirement.

Better results are obtained if the battery initial voltage and SOC is larger (SOC= 0.8), as they are shown in Fig. 17. A little larger terminal voltage makes the difference. This simulation results prove that a battery storage energy system is a better solution than a super- capacitor whose terminal voltage variation has to be much larger (50% to tap 75 % of its stored energy).

This would triggers the necessity of higher initial voltage to produce enough large electric power during vehicle braking.

7. Extension of IPM Alternator utilization up to 100 kW Systems

Based on the same optimization program used in the analysis of the 8 kW braking power IPM-CPA, we have studied also the possibility of obtaining Claw Pole Alternators up to 100 kW. The study was made on the IPM-CPA with the following powers: 5, 10, 25, 50 and 100 kW. The idea is that at this range of powers the claw pole machine could be used also as a starter / alternator with full inverter control. The evolution of the main dimensions can be seen in Table II. It seems that the IPM-CPA is fully competitive with alternative electric propulsion systems up to 100 kW on automobiles.

Table 2.
Dimensions evolution of the IPM-CPA

	Power [kW]				
	5	10	25	50	100
U [V]	40	42	250	500	500
η [%] at $6 \cdot 10^3$ [rpm]	85	89	93	95	95
Total mass [kg]	7.5	13	43	59	62
hag [mm]	0.4	0.85	0.85	0.9	1.2
sDo [mm]	163	195	300	370	375
sDi [mm]	107	145	230	300	308
lc [mm]	35	47	52	52	49

8. Conclusion

This paper presents an optimization design study (based on MEC model and Hooke-Jeeves modified algorithm) and a 3D-FEM study of the IPM-CPA. Clear improvements of the efficiency, output power and flux are presented.

The proposed vehicle “hidden” 42 Vdc power net modeling and simulations show that recovering a good part of breaking energy is a feasible solution to increase the vehicle energetic efficiency and for emission reduction in classical power train vehicles.

The proposed system and component model could be used as a tool to study the system behavior and for control strategy optimization.

New control options regarding charging recharging current level while considering the battery SOC and load power could also be developed. The presented simulations show that a battery storage solution is better than a super-capacitor storage solution due to smaller voltage regulation range in the former.

Acknowledgement

This work is part of European FP7 EE-VERT 2009-2011 program regarding the possibility of building a more efficiently automobile. Thank are to Robert Bosch GmbH for providing the experimental alternator data.

Also, this work was partially supported by the strategic grant POSDRU/89/1.5/S/57649, Project ID 57649 (PERFORMERA), co-financed by the European Social Fund – Investing in People, within the Sectoral Operational Programme Human Resources Development 2007-2013.

References

1 Boldea, I., The electric Generators Handbook - *Variable Speed Generators*, book, CRC Press, Taylor and Francis Group ,New York, 2006.

2 Schule, St., Hameyer, K., *Computational of the mutual inductance between Rotor and Stator of Synchoronous Claw-Pole Alternators regarding Claw Chamfers*, Electrical Machines and drives, 2005, IEEE International conference on, pp.1300-1303,2005.

3 Guo, Y. G. , Zhu,J. G. ,*Design and analysis of a three-phase three-stack claw pole permanent magnet motor with SMC stator*, Paper 85, Proceedings of Australasian Universities Power Engineering Conference (AUPEC 2003).

4 Perreault, D. J. , and Caliskan,V., *Automotive power generation and control*, IEEE Transaction on power electronics, vol. 19, NO.3,pp. 618-630, May 2004.

5 Li L., Kedous-Lebouc, A., FoggiaA. , and Mipo,J.C., *Influence of magnetic materials on claw pole macine behavior*, IEEE Trans. On Magnetics vol. 46, issue 2, pp 574-577, 2010.

6 J. G. Kassakin, H. C. Wolf, J. M. Miller, C. J. Hurton; *Automotive Electrical Systems Circa 2005; Demands for Better Fuel Economy and more Electric Power are Driving Cars to Multiple Higher Voltages*; IEEE Spectrum, AUGUST 01, 1999, pp. 12

7 Perreault, D.J., Keim, T. A, Lang, J. H. , and Lorrila, L. M., *Applications of power electronics in automotive power generation*, Automotive power electronics- Paris ,21-22 June,2006 .

8 Chung, S., Keim, T. A., and Perreault,D.J.,*Thermal modeling of Lundell Alternators, IEEE Trans on Energy conversion*, vol. 20, No.1, march 2005.

9 Krahenbruhl, D., Zwyssig, C., Kolar, J.K., *Half-Controlled Boost Rectifier for Low_Power High-Speed Permanent-Magnet Generators*, IEEE Trans on Industrial Electronics, vol. 58, No.11, Nov. 2011, pp. 5066-5075.

10 Whaley, D.M., Soong,W.L. , and Ertugrul,N., *Extracting more power from the Lundell car alternator*, presented at the Australian Univ Power eng conf. AUPEC, Brisbane, Australia, 2004

11 J. G. Kassakin, H. C. Wolf, J. M. Miller, C. J. Hurton; *Automotive Electrical Systems Circa 2005; Demands for Better Fuel Economy and more Electric Power are Driving Cars to Multiple Higher Voltages*; IEEE Spectrum, AUGUST 01, 1999, pp. 12

12 Giorgetti, F. Pastena, L. Tarantino, A. Velotto, F.; *Energy saving by onboard storage; Power Electronics, Electrical Drives, Automation and Motion*, 2006. SPEEDAM 2006. International Symposium on, Taormina, 23-26 May 2006, pp. 481 – 483;

13 B. Simpkin, R. Marco, C. D'Ambrosio, M. Abele, G. Heuer, A. Ferré, I. Boldea, S. Scridon, *Improved Energy Efficiency For Conventional Vehicles Through An Enhanced Dual Voltage Architecture And New Components With An Attractive Cost-Benefit Ratio*, EVER, Monaco, 31 March-3 April, 2011, paper 70.

14 Kessels J.T.B.A.; Koot, M.; de Jager, B.; van den Bosch, P.P.J.; Aneke, N.P.I.; Kok, D.B.; *Energy Management for the Electric Power net in Vehicles With a Conventional Drivetrain; Control Systems Technology*, IEEE Transactions on, May 2007, Volume: 15 Issue:3, pp. 494 – 505;

15 Szenasy, I.*; New energy management of capacitive energy storage in metro railcar by simulation*; Vehicle Power and Propulsion Conference, 2009. VPPC '09. IEEE, 7-10 Sept. 2009, pp. 181 – 187;

16 Rajashekara, K.; *42 V architecture for automobiles*; Electrical Insulation Conference and Electrical Manufacturing & Coil Winding Technology Conference, 2003. Proceedings, pp.431-434;

17 Sai Chun Tang; tten, D.M.; Keim, T.A.; Perreault, D.J.; *Design and Evaluation of a 42-V Automotive Alternator With Integrated Switched-Mode Rectifier*, Energy Conversion, IEEE Transactions on, Dec. 2010,Vol. 25 Issue:4, pp. 983 – 992;

18 Naidu, M.; Nehl, T.W.; Gopalakrishnan, S.; Wurth, L. *A semi-integrated sensorless PM brushless drive for a 42 V automotive HVAC compressor* Industry Applications Conference, 2003. 38th IAS Annual Meeting. Conference Record of the Volume: 3, 2003, Page(s): 1435 - 1442 vol.3

19 Sung-Il Kim; Geun-Ho Lee; Jung-Pyo Hong; Tae-Uk Jung;*Design Process of Interior PM Synchronous Motor for 42-V Electric Air-Conditioner System in Hybrid Electric Vehicle* Magnetics, IEEE Transactions on Volume: 44 , Issue: 6 Digital Object Identifier: 10.1109/TMAG.2007.916136: 2008 , Page(s): 1590 – 1593

20 Ostovic, V., Miller, J.M., Garg,V., Schultz, R.D., Swales, S., *A magnetic equivalent circuit based performance computation of a Lundell alternator*, IEEE Trans. On Industry Applications, vol.35, issue 4, pp.825-830, 1999.

21 Ostovic, V., *Dynamics of saturated machine* , book, Springer – Verlag, New York, 1989

22 Boldea, I., Tutelea, L., *Electric machines: steady state, transients, testing &design, with MatLab*, book,CRC Press, Taylor&Francis Group,N.Y. 2009

23 Bianchi, N. , *Electrical machine analysis using finite elements*, book, CRC Press, Taylor and Francis Group, Boca Raton, 2005

24 Opera-3D User Guide,VF-12-09-D2, Vector Fields software, 24 Bankside , Oxford OX5 1JE, England

25 Vahe Caliskan, David J. Perreault, ThomasM. Jahns, John G. Kassakian; *Analysis of Three –Phase Rectifiers with constant –voltage loads*; IEEE Transactions on circuit and systems; vol. 50, No. 9, September 2003 pp.1220-1226;

26 Hua Bai, Steven D. Pekarek, Jerry Tichenor, Walter Eversman, Duane J. Buening, Gregory R. Holbrook, Michael L. Hull, Ronald J. Krefta Steven J. Shields, *Analytical Derivation of Coupled-Circuit Model of a Claw Pole Alternator With Concentrated Stator Windings*; IEEE Transactions on Energy Conversion, vol. 17, no. 1 March 2002, pp. 32-38;